Journal of Structural Geology, Vol. 12, No. 2, pp. 273 to 282, 1990
Printed in Great Britain

0191-8141/90 $03.00+0.00

The effect of initial perturbation shape and symmetry on fold development

MOHAMMAD R. ABBASSI and NEIL S. MANCKTELOW

Geologisches Institut, ETH-Zentrum, CH-8092 Zürich, Switzerland

(*Received* 23 *January* 1989; *accepted in revised form* 24 *July* 1989)

Abstract—Single-layer fold experiments were carried out to study the influence of initial perturbation symmetry on the symmetry of folds developed using paraffin wax as a rock analogue. Under experimental conditions, both matrix and layer have a power-law rheology, with an initial effective viscosity contrast of *ca* 17:1. The matrix flows in steady state with $n = 2.7$ and the layer work softens with $n_{eff} \approx 10$. Folds developed from an initially symmetric perturbation remain symmetric, reflecting the pure shear–plane strain boundary conditions. Folds developed from an initially asymmetric perturbation, however, show a progressive exaggeration of this asymmetry, such that the introduced 3.5° difference in limb dip increases to 65° at 23% bulk shortening. These experiments indicate that, for low competence contrast between layer and matrix, the geometry of initial perturbations of finite amplitude (e.g. ripple marks, channels, half-graben structures) may be an important factor in determining the geometry and distribution of folds.

INTRODUCTION

THE existence of random, minor perturbations in the original 'planar' layer, which can be selectively amplified to form folds, is implicit in all theories of single-layer buckle folding (Biot 1957, 1959a,b, 1961, Ramberg 1963, Fletcher 1974, 1977, Smith 1975, 1977, 1979). If larger, non-random perturbations are present within such a layer, however, the shape of this initial perturbation may influence the wavelength (Williams *et al.* 1978), amplitude (Biot *et al.* 1961, fig. 5) and shape (Chapple 1968) of the folds developed. This effect should be most apparent for low competency contrast between layer and matrix, when the wavelength selectivity of the buckling mechanism is low (e.g. Biot 1961). The growth rate of the theoretical dominant wavelength may then be insufficient to outpace the amplification of initial perturbations of larger amplitude and different wavelength.

The effect of isolated perturbations on fold development has been investigated analytically by Biot *et al.* (1961), numerically by Williams *et al.* (1978) and experimentally by Cobbold (1975). Cobbold (1975) showed that the development of fold packets within otherwise planar, homogeneously shortened layers was controlled by the presence of initial irregularities. He suggested that, in nature, laterally continuous fold trains may develop by sideways propagation and mutual interference between fold packets initiated at many perturbation sites. This concept differs fundamentally from the more common models of folding, which assume selective amplification of randomly distributed, very small, periodic perturbations with a broad range of initial wavelengths (cf. Biot 1961, Ramberg 1963, Fletcher 1977, Smith 1979). In these models, the fold train develops instantaneously along the full length of the layer and does not involve sideways propagation from individual sites.

Asymmetric folds are generally considered to form by compression oblique to the layer (e.g. Treagus 1973), by bulk non-coaxial flow (Ghosh 1966, Manz & Wickham 1978, Casey & Huggenberger 1985) or by the development of asymmetric parasitic folds during polyharmonic folding (e.g. Ramsay & Huber 1987, fig. 20.1). The study discussed here investigates how the symmetry of individual initial perturbations, which initiate folding, can control the symmetry of the folds developed. The scale-model experiments were designed to test the hypothesis that asymmetric folds may in some cases develop through the amplification of an initially asymmetric perturbation shape, and may not necessarily reflect an asymmetric orientation of the layer relative to the shortening direction. This could be directly applicable to many natural examples, as irregularities in the original bedding surface often show a systematic asymmetry (climbing ripples, asymmetric ripple marks, flute casts, etc.), and such asymmetric pre-tectonic irregularities also occur on the regional scale (e.g. syn-sedimentary half-grabens). Non-systematic initial perturbation asymmetry could result in irregular variation in fold asymmetry along a single layer.

EXPERIMENTAL PROCEDURE

If the effects of body forces (gravity, inertia) in both the model and the natural original can be ignored, the model ratios of time, length and force are mutually independent (Hubbert 1937, Cobbold 1975, Ramberg 1981), but must be uniform throughout the model. Under these assumptions, model ratios can be chosen which best suit the experimental conditions. The one important restriction is that there must be rheological similarity between the original rock and the analogue modelling materials (Cobbold 1975, Weijermars & Schmeling 1986, Mancktelow 1988b).

Experimental conditions

The scale-model experiments were conducted with boundary conditions of confined plane strain–pure shear using the deformation rig described by Mancktelow (1988a). The experiments were performed at a constant natural strain rate of $3 \times 10^{-5}\,s^{-1}$, at a temperature of 27 ± 0.1°C and with a confining stress σ_3 of 0.3 bar (0.03 MPa).

Modelling materials

Paraffin waxes were chosen as our non-linear modelling materials. These waxes display power-law stress–strain rate behaviour under experimental conditions (Mancktelow 1988b) and are rheologically similar to the predicted behaviour of many rocks during natural deformation (e.g. Tullis 1979). The highly refined waxes were obtained from major chemical suppliers (see appendix of Mancktelow 1988b). The single competent layer was constructed from wax of melting range 58–60°C, the weaker matrix from wax of melting range 46–48°C.

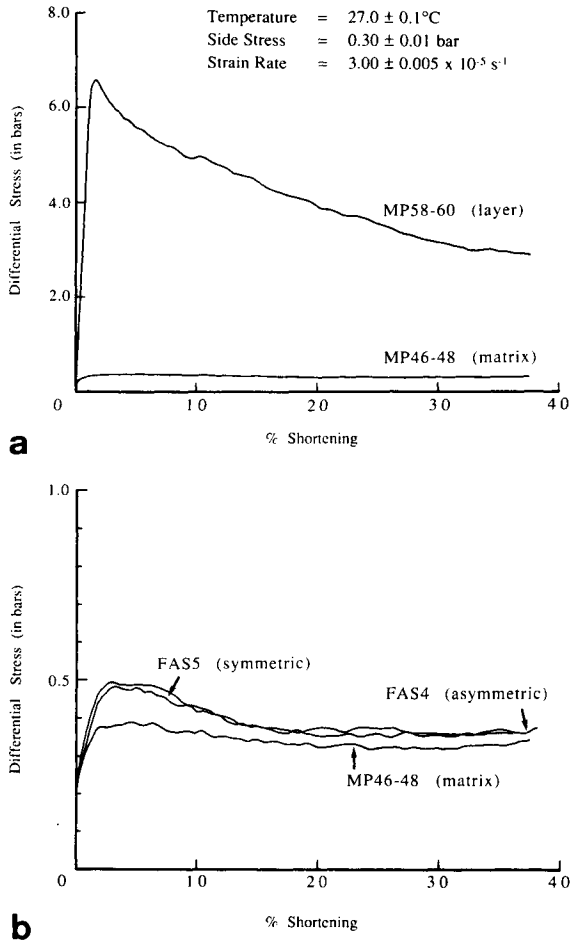

Fig. 1. Differential stress (bars) vs strain (as % shortening) curves for the model materials under experimental conditions. (a) Calibration curves for single blocks of the matrix wax MP46–48 (melting range 46–48°C) and of the wax MP58–60 (melting range 58–60°C) used to construct the stiffer layer. (b) Stress–strain curves recorded during the folding experiments FAS4 and FAS5. Note that the stress–strain curves are practically identical and independent of the symmetry of the initial perturbation. The calibration curve for the matrix wax alone (MP46–48) is included for comparison.

Under the chosen experimental conditions, the matrix wax flows at nearly steady state (Fig. 1), with a power-law constitutive relationship between natural strain rate $\dot{\varepsilon}$ (in s^{-1}) and differential stress σ (in bars) of the form:

$$\dot{\varepsilon} = A \exp(-Q/RT)\,\sigma^n$$

with calibrated values for the constants of

$$A = \exp(204)$$

$$Q = 126\ \text{kcal mol}^{-1}$$

$$n = 2.7.$$

Further details can be found in Mancktelow (1988b). The stiffer wax used to construct the layers is work-softening under the same conditions (Fig. 1) and a constitutive relationship independent of ε is not possible. For our experimental conditions, the ultimate strength of the layer is 17.2 times the flow stress of the matrix wax (Fig. 1).

Perturbation and layer geometry

The initial perturbations were introduced as single arcs on an otherwise 'planar' layer. The symmetric perturbation had initial limb dips of 6°, an amplitude of 0.75 of the layer thickness and, to a first approximation, a bell-like shape (cf. fig. 2 of Biot *et al.* 1961); the asymmetric perturbation had limb dips of 4.5° and 8°, respectively, and an amplitude of 0.64 of the layer thickness. The initial bonding between layer and matrix was weak, corresponding to the assumption of easy slip between layer and matrix in folding theories (e.g. Biot 1959b, 1961).

EXPERIMENTAL RESULTS

Fold shape

It is very obvious from a comparison of the photographic records for the two experiments in Fig. 2 that the fold initiated on an asymmetric perturbation (FAS4) develops an exaggerated asymmetry at high fold amplitudes. The asymmetry is also very marked in the heterogeneous strain distribution in the immediately surrounding matrix, as is seen in a plot of the long axes of the finite-strain ellipses at 23% shortening (Fig. 4a) and the trajectories constructed parallel to these axes (Fig. 4b). This is particularly marked within the highly strained, inner arcs of the folds.

This asymmetry in the matrix deformation diminishes rapidly away from the layer, however. This can be seen directly in the photographic record (Fig. 2b), where the displacement of the grid lines is approximately symmetric only a short distance from the strongly asymmetric fold in the layer, and likewise from the plots of Fig. 4. It can also be seen from Fig. 4(b) that the location of the low strain, triangular zone within the matrix on the outer arc of the folds (cf. Ramsay & Huber 1987, fig. 21.23) is similar in the two experiments. Its location and form

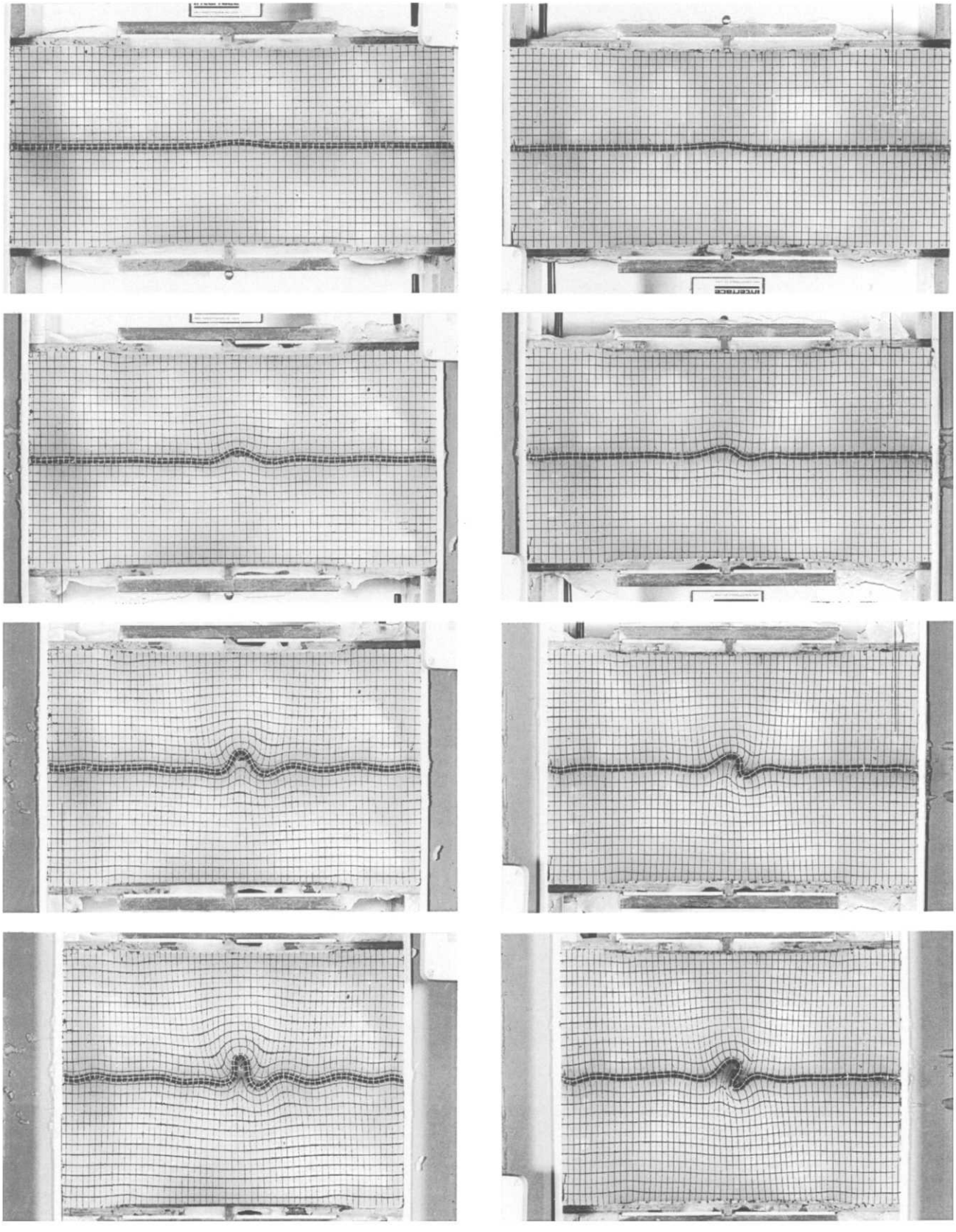

Fig. 2. Photographic record of the symmetric experiment FAS5 (a), and the asymmetric experiment FAS4 (b). In both cases, the photographs were taken at 0, 8, 16 and 23% shortening and the initial layer thickness was 4 mm.

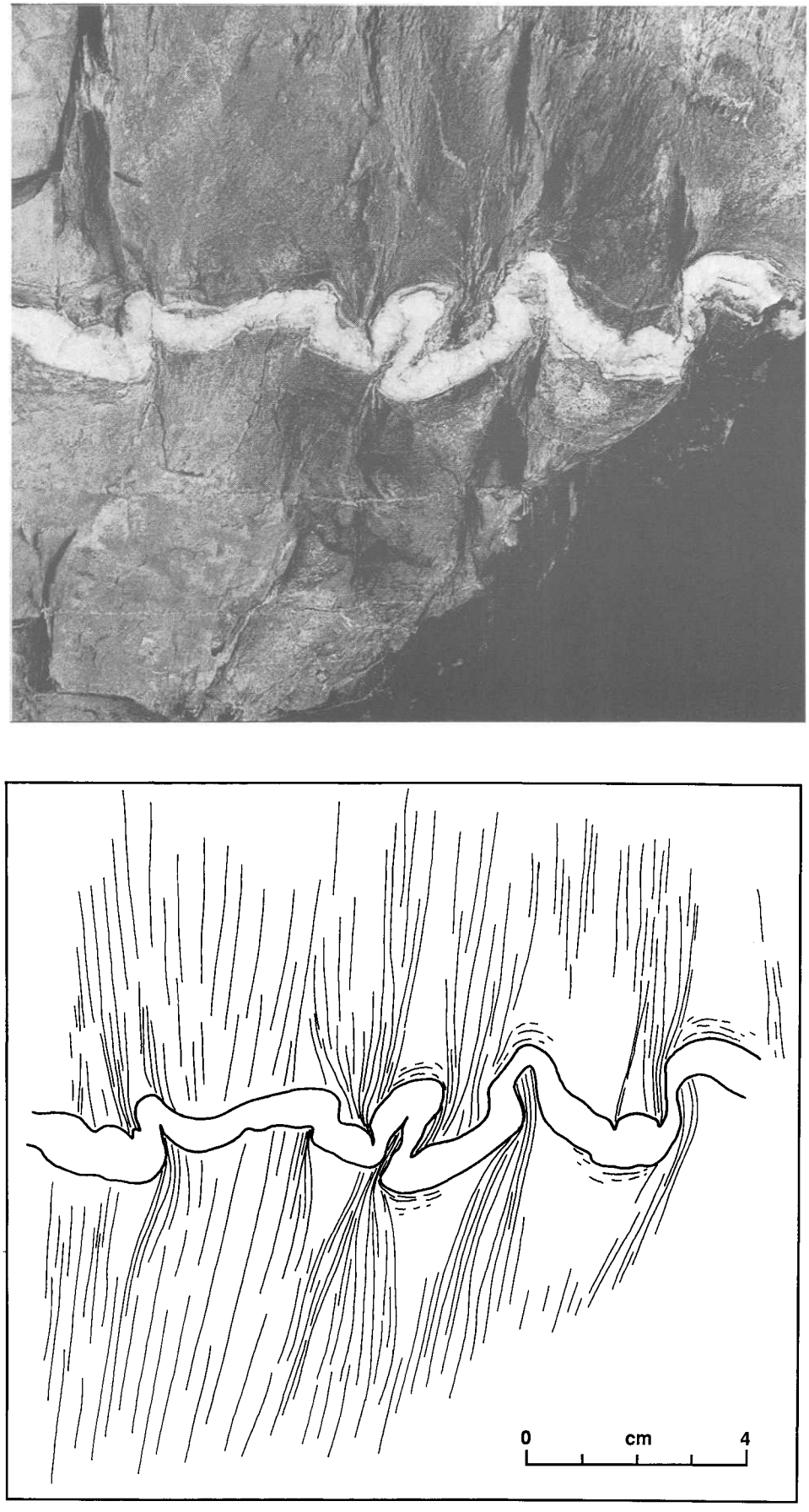

Fig. 3. Natural example of irregular asymmetric folding (calcareous flysch from Cinque Terra, Italy). The folded layer is a white calcite vein of coarser grain size than the calcite in the matrix of calcareous shale. The geometry of layering and cleavage, as emphasized in the line drawing, can be compared directly with the strain trajectories of Fig. 4(b).

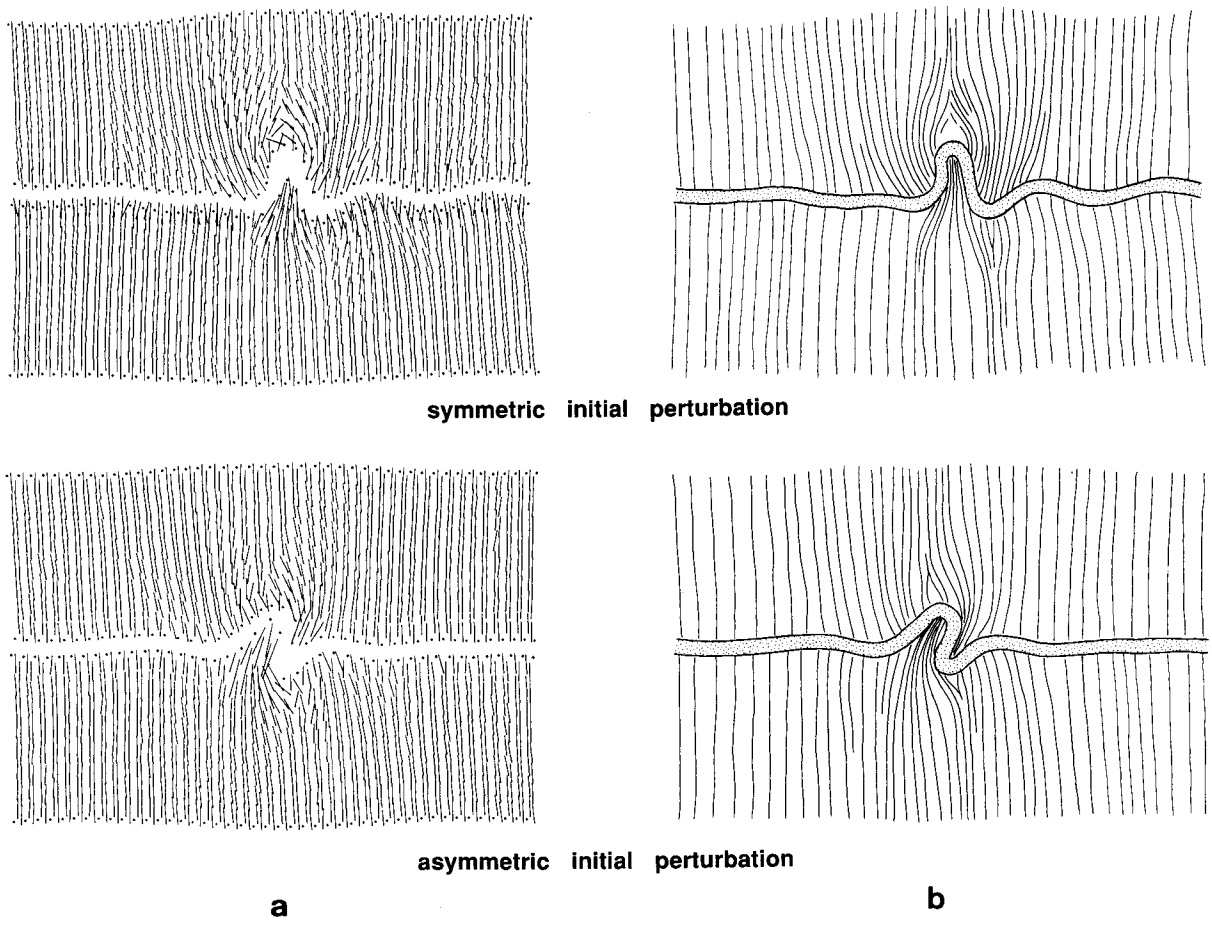

Fig. 4. (a) Plot of the long axes of the finite-strain ellipses at 23% shortening for the symmetric and asymmetric experiments. (b) Trajectories parallel to the axes of (a). This pattern may be directly compared with the cleavage pattern in natural examples to check for correspondence.

appear to be largely determined by the bulk strain. As a result, it is displaced with regard to the axial plane of the asymmetric fold. A similar geometry was observed for folds developed experimentally during simple shear by Manz & Wickham (1978). This characteristic pattern does not, therefore, allow a distinction between the effects of initial perturbation geometry and rotational boundary conditions.

The folding of the layer itself can be analysed in more detail by considering the history of limb dip at the inflection points. This is presented as a plot of limb dip against percent shortening for the symmetric case in Fig. 5(a) and the asymmetric case in Fig. 5(b). Curves calculated for the dip of the limb segments, had they behaved as passive material lines in a homogeneous deformation, are also presented for comparison. The marked differ-

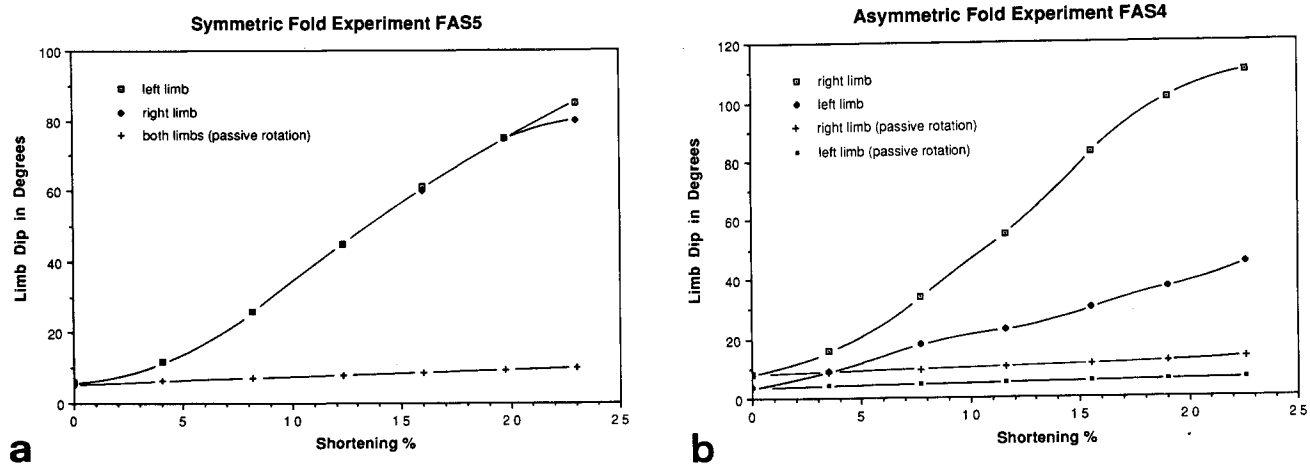

Fig. 5. Dips of the two limbs (measured at the inflection points) of the central fold developed from the initial perturbation, plotted against the percent shortening. The calculated curve for the orientation of these limbs, had they behaved as passive material lines in a homogeneously deforming matrix, is also given. (a) Symmetric initial perturbation (experiment FAS5). (b) Asymmetric initial perturbation (experiment FAS4).

ence between the calculated and the observed behaviour represents the effect of the mechanical instability. The two limbs of the initially symmetrical perturbation behave identically and, therefore, maintain the symmetry of the central fold throughout the experiment (Fig. 5a). In contrast, the initial difference in the dip of the two limbs of the asymmetric perturbation is greatly amplified during deformation (Fig. 5b), from 3.5° at 0% to 65° at 23% shortening. The asymmetry has been markedly accentuated by the deformation, even though the boundary conditions of the experimental deformation are symmetric and coaxial.

Fold propagation

The progressive distribution of the fold train along the layer, by sideways propagation away from the initial perturbation, is slow. Shortening of the stiffer layer by folding is largely restricted to the central region around the perturbation (Fig. 2). Indeed, the rate of propagation appears to be less than the already limited rate in the experiments of Cobbold (1975). This may be influenced by the degree of bonding between layer and matrix. In our experiments the degree of bonding was weak, and the preferential folding at one site on the layer around the initial perturbation is accommodated by displacement of the layer relative to the matrix in the straighter segments to either side. In contrast, Cobbold (1975) attempted to achieve a high degree of bonding, slip between layer and matrix was more difficult, and the fold train propagated laterally more rapidly. It appears that strong and even bonding between layer and matrix promotes the development of a more regular fold train. The low rate of sideways propagation may also be due to the strain-softening behaviour of the stiffer layer, which would tend to promote strain heterogeneity by preferentially accommodating strain within already strongly strained material. In contrast, both matrix and layer flowed at nearly steady state in the experiments of Cobbold (1975).

Layer-parallel shortening

The amount of layer-parallel shortening was calculated as:

$$\% \text{ layer shortening} = \frac{l_0 - l_1}{l_0} \times 100\%,$$

where l_0 and l_1 are the initial and deformed arc lengths measured from end-to-end along the layer (e.g. Hudleston 1973). The results are presented in Fig. 6, plotted against the bulk shortening as determined for a straight line joining the ends of the layer. There is a remarkable degree of consistency, which was not entirely expected considering the markedly different end geometries. A third-order polynomial provides a nearly perfect fit to the data points of experiment FAS5 (the symmetric perturbation), and the first- and second-order derivatives of this fitted curve are plotted in Fig. 7. From this plot it is clear that layer-parallel shortening is initially

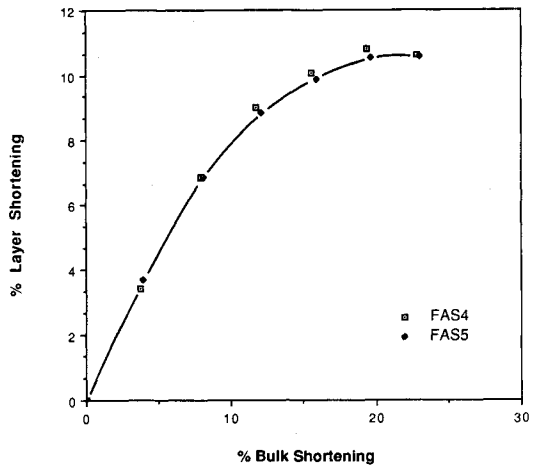

Fig. 6. Plot of layer-parallel shortening vs bulk shortening for both experiments. The curve is a third-order polynomial best-fit to the data from experiment FAS5. The first- and second-order derivatives of this curve are used in Fig. 7.

the overwhelming mechanism by which bulk shortening of the layer is accomplished (first derivative ≈1 at 0%), but that it steadily loses in influence, until at around 20% bulk shortening it is insignificant (cf. Hudleston 1973).

Fold amplification

The two experiments discussed here were designed to evaluate the influence of perturbation geometry and not specifically to investigate the selection and growth of a dominant wavelength within a buckled layer. The initial perturbations are of finite amplitude, with introduced limb dips ≥5°, and thus beyond the scope of conventional infinitesimal-amplitude treatments (Chapple 1968). With this limitation in mind, however, the results can still be compared with many previous theoretical and experimental studies on fold initiation and amplificaion (e.g. Biot 1961, Sherwin & Chapple 1968, Hudleston 1973, Fletcher 1974, Cobbold 1975, Smith 1979, Neurath & Smith 1982).

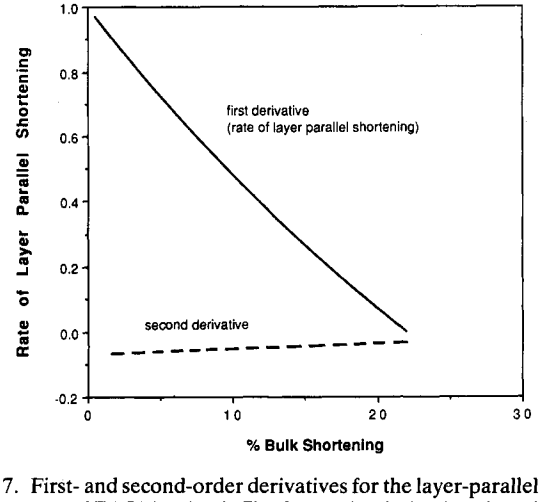

Fig. 7. First- and second-order derivatives for the layer-parallel shortening curve of FAS5 in Fig. 6. The first-order derivative gives the rate of layer-parallel shortening: a value of 1 indicates that all the bulk shortening can be accommodated by layer-parallel shortening, a value of 0 that none of it is.

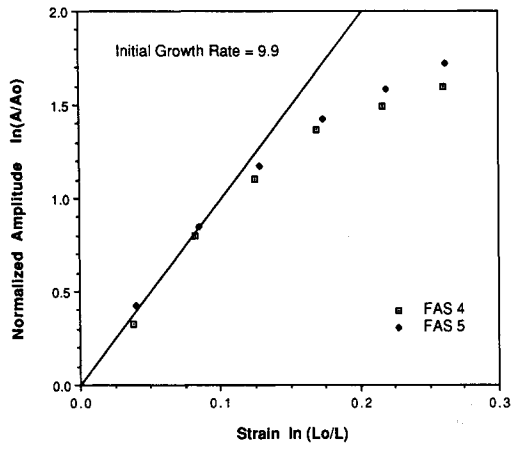

Fig. 8. Amplitude of the central fold developed from the initial perturbation in the two experiments FAS4 and FAS5. The slope of the curve at any point represents the growth rate at that value of natural strain. The initial growth rate is effectively constant to *ca* 10% shortening, with a value of about 10.

Following Smith (1977) and Neurath & Smith (1982), the normalized growth rate, γ, is defined as $(dA/A) = -\gamma(dL/L)$, where A is the disturbance amplitude and L is the length of a passive marker line far from and parallel to the layer (≡ to the length of the model parallel to the layer). On integration, this becomes $\ln(A/A_0) = \gamma \ln(L_0/L)$. To obtain γ, we plot $\ln(A/A_0)$, i.e. the natural log of the normalized amplitude, against $\ln(L_0/L)$, which is $-\varepsilon$ (the natural or logarithmic strain). The slope of this curve at any point will equal the growth rate as defined above. It is immediately clear from Fig. 8 (and also from fig. 6 of Neurath & Smith 1982), that this plot is only linear at very low strains ($-\varepsilon < 0.1$, ≈10% shortening), corresponding to limb dips of the central fold of less than 30° (Fig. 5); within this linear range the growth rate of the initial perturbation is approximately 10. As can be seen from the summary plot of Fig. 9, the results are broadly consistent with the earlier experiments of Cobbold (1975) and Neurath & Smith (1982). The growth rate in our experiments is, however, lower than expected from the relevant non-linear fold theory (Fig. 9). There are probably two factors contributing to this observation. Firstly, the growth rates determined in all these experiments (including those of Cobbold 1975 and Neurath & Smith 1982) were measured on finite-amplitude folds developed from small but finite initial perturbations. These rates may be consistently lower than the initial growth rate within the scope of the infinitesimal-amplitude theoretical treatments (limb dip <5°), where direct experimental measurement is impractical. Secondly, as noted by Biot *et al.* (1961), the growth rate of the central fold developed from an initial bell-shaped perturbation with average wavelength longer than the theoretical dominant wavelength (i.e. our case), is less than the growth rate of an initial perturbation with average wavelength equal to the theoretical dominant wavelength. This effect becomes more marked as the competence contrast between layer and matrix decreases (Biot *et al.* 1961, fig. 5), and may be further influenced by the observed layer-parallel shortening.

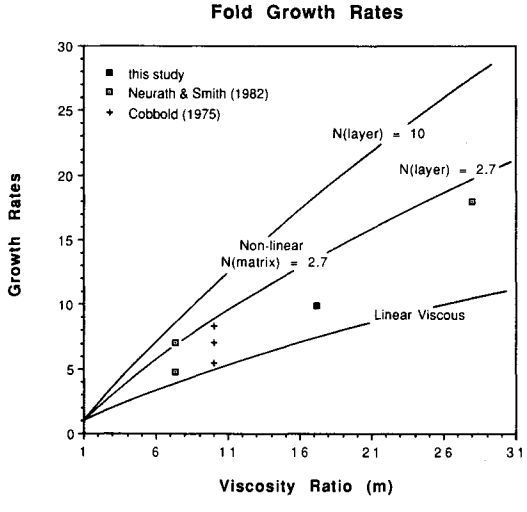

Fig. 9. Summary of published results on experimental growth rates of folds (based on the collation in tables 2 and 3 of Neurath & Smith 1982). The solid curves give the theoretical initial growth rates for folds in linear viscous materials and for non-linear materials with effective stress exponents $n_1 = 2.7$ (matrix) and $n_2 = 2.7$ and 10 (layer) using the equations of Fletcher (1974) and Smith (1979).

Wavelength selection

The wavelength of folding has been determined in two ways: by Fourier spectral analysis and by measuring the *average fold arc lengths* (Sherwin & Chapple 1968, Hudleston 1973, Fletcher & Sherwin 1978). The results are listed in Table 1. The internal consistency between the two experiments is remarkably good, and indicates an initial preferred wavelength to layer thickness ratio of around 10. The imposed boundary conditions demand the development of an integer number of half-folds within the layer length, because the ends of the layer represent fixed nodes. This, of course, places restrictions on the possible values of N in Table 1, and restricts the accuracy of our wavelength determination. In summary, the design of the current experiments does not allow a rigorous study of the wavelength selection process, but suggests a preferred wavelength to thickness ratio of *ca* 10.

Table 1. Average fold arc lengths for the two experiments, defined as the total arc length measured along the layer (L) divided by the number of folds (N) and normalized against the layer thickness (d). Values were calculated at initiation (0%) and at 23% shortening; the difference reflects the layer-parallel shortening (and consequent layer thickening) during the experiments. The dominant wavelength was also estimated by Fourier spectral analysis. Power spectra were calculated at intervals of *ca* 4% bulk shortening (to 23%, cf. Fig. 2), allowing a projection of the maximum amplitude fold component towards a limit of 0% strain to determine an initial dominant wavelength; these are the values given in the table

Experiment	No. of folds (N)	$L_{0\%}/N/d_{0\%}$	$L_{23\%}/N/d_{23\%}$	Fourier
FAS4	7	10.2	8.1	9.1
FAS5	7	10.8	8.6	10.8

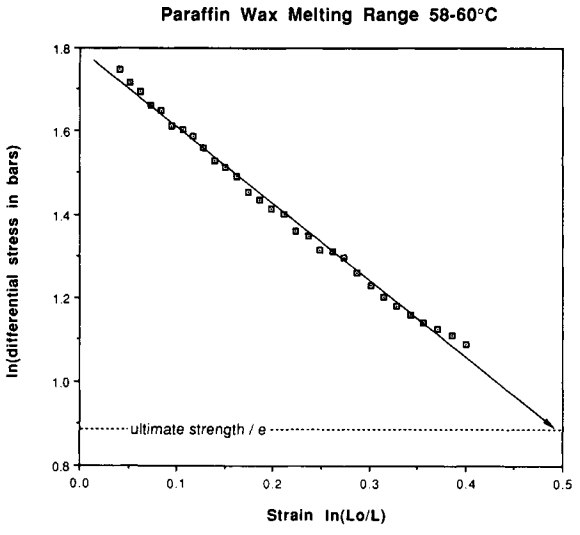

Fig. 10. Strain softening behaviour of wax MP58–60 (the material used to construct the stiff layer in the model experiments), shown as a plot of natural log differential stress (in bars) vs natural strain. A linear plot would represent an exponential decay of flow stress with strain. The value ε^* is the strain at which the stress falls to 1/e of its initial value (i.e. the ultimate strength).

As discussed above, our model materials are not linear-viscous, but follow a power-law relationship. For the experimental conditions employed, the matrix flows at near steady state, whereas the competent single layer shows significant strain softening (Fig. 1). Neurath & Smith (1982) proposed an extension of the theory of buckling instability in non-linear materials to strain-softening materials. For simplicity, they assumed an exponential decay of flow stress with strain, which appears to be approximately true for the stiff paraffin wax used for the layers in our experiments (Fig. 10). They defined a measure of the degree of strain softening, ε^*, as the strain at which the deviatoric flow stress drops to (1/e) of its initial value. Linear regression of the data in Fig. 10 gives a value of $\varepsilon^* \approx 0.5$. Neurath & Smith (1982) concluded that the combined effect of strain and strain-rate softening can be characterized by defining an effective power-law exponent, which is dependent on both ε^* and the growth rate γ:

$$\frac{1}{n_{\text{eff}}} \equiv \frac{1}{n} - \frac{2}{\sqrt{3}\gamma\varepsilon^*}.$$

The second term in this equation gains in significance for slow growth rates (i.e. low competence contrast between layer and matrix) and low ε^* (strongly work-softening materials). Substituting values of 10 for γ (see the section on fold amplification above), 0.5 for ε^*, and 3 for the stress exponent n, the effective power-law stress exponent for our stiffer wax would be around 10.

With this value for the exponent in the competent layer and a value of 2.7 for the matrix, the non-linear theory of Fletcher (1974, 1977) and Smith (1975, 1977, 1979) would suggest a dominant wavelength to thickness ratio of about 6, compared with a value of around 9 for linear viscous materials (Biot 1961). In our experiments, folds developed with initial normalized wavelengths of around 10, which is somewhat longer than the dominant wavelength predicted by the non-linear theories. Williams *et al.* (1978) found that in their finite-element simulations of linear viscous folding, the selected wavelength was always greater than that predicted by Biot when the introduced initial perturbation was of wavelength significantly longer than the theoretical dominant wavelength. The fold never attained the wavelength characteristic of the viscosity ratio and indeed the whole development of the fold depended on the initial perturbation. This may be directly compared to our experiments, where the initial, non-periodic perturbation has an arc length of *ca* 11.5 times layer thickness (i.e. a 'wavelength'/*d* ratio of *ca* 23), which is clearly much larger than the expected (and observed) dominant wavelength.

NATURAL EXAMPLES

Measurement of natural folds gives low wavelength to thickness ratios, usually <10 and commonly in the range 4–6 (e.g. Sherwin & Chapple 1968, table 1, Smith 1979, table 1). This implies a correspondingly low effective viscosity ratio between layer and matrix (≪50) and non-linear material behaviour to achieve the amplification of the observed folds (Smith 1979, fig. 3). For such natural conditions, the influence of the geometry of the initial irregularities in the layers may be significant, particularly since natural irregularities are often non-random in their geometry and distribution.

Not all natural folds show a simple and regular periodicity. Indeed, many are quite irregular in their wavelength, amplitude and geometrical form (e.g. Fletcher & Sherwin 1978, fig. 1). An example of such a wave train within a single layer is shown in Fig. 3. The cuspate–lobate fold form (cf. Ramsay & Huber 1987, figs. 19.14–19.16), together with the low wavelength to thickness ratio (≈9–10) suggest a rather low effective viscosity contrast between layer and matrix during folding. The orientation of the axial plane varies from fold to fold, while the cleavage away from the folded layer is near planar, constant in orientation and perpendicular to the layer; the overall shortening was approximately parallel to the layer. It is obvious in this natural example, therefore, that the geometry of each fold is controlled by some factor intrinsic to that individual fold (presumably the initial perturbation geometry) rather than an extrinsic factor such as the bulk-strain geometry. The natural cleavage pattern of Fig. 3 may be directly compared with the strain trajectory pattern of the asymmetric fold experiment (FAS4) in Fig. 4(b). The characteristics are very similar: variability in cleavage orientation is only developed in the immediate vicinity of the asymmetric folds and particularly on the inner arcs, while the triangular, low strain zones on the outer arcs maintain a relatively symmetrical distribution.

For more regular natural fold trains, the influence of periodic initial irregularities on the buckling behaviour is more difficult to determine. The control of fold geom-

ometry by pre-existing structures may in some cases be established by direct observation, for example if synformal hinges always correspond to the base of scour channels. However, this may not always be possible, as the initial irregularities may have been quite small, but still significant in initiating folding.

CONCLUSIONS

The experiments demonstrate that, for relatively low competence contrast (*ca* 17:1 in this study), the symmetry of small initial irregularities in the layer may control the symmetry of the folds developed, independently of the bulk-strain geometry. As the result of shortening parallel to the layer of 23%, an initial minor asymmetry in limb dip of only 3.5° was exaggerated to 65°. This marked asymmetry in the folded layer is reflected in the strain distribution within the immediately adjacent matrix, but this asymmetry diminishes rapidly away from the fold. The experiments also emphasize the importance of isolated irregularities in localizing the site of fold initiation (cf. Biot *et al.* 1961, Cobbold 1975). The observed propagation of the fold train along the layer is relatively slow, such that the fold packet remains concentrated around the site of the initial perturbation. This may be exaggerated in our experiments by the strain softening behaviour of the layer material, tending to preferentially accommodate further strain increments within the already strained region. Rock mechanics experiments suggest that the complete range of strain-dependent behaviour, from strain hardening, through steady-state, to strain softening may occur in rocks under different geological conditions (e.g. the review of Tullis & Tullis 1986). This could be reflected in the folding behaviour of single layers, from a tendency to strain homogenization in strain hardening materials, with lower fold amplification rates and rapid layer-parallel propagation of fold trains, to marked strain concentration for strain softening materials, resulting in rapid amplification and the concentration of folding in packets surrounding initial perturbations.

As expected for low competence contrast conditions, layer-parallel shortening during folding is also significant, reaching values of around 10% at 25% bulk shortening. The deformation of the layer clearly cannot be divided into a discrete two stage history of initial layer parallel shortening followed by folding of a layer of constant thickness. The change in layer length occurs progressively during folding, but diminishes in relative importance as deformation proceeds (Fig. 6). Similar experimental observations were made for folds in linear materials by Hudleston (1973).

Many natural, single-layer folds have a geometry and wavelength indicative of low competence contrast folding (e.g. Sherwin & Chapple 1968); as is clear from the current experiments, the symmetry and distribution of folding within such layers will be strongly controlled by any initial, non-random irregularities of finite size. Such irregularities are particularly common as sedimentary structures in bedding, and their influence on folding during natural deformation may be widespread.

Acknowledgements—Thanks to John Ramsay for his initiation and support of the Model Deformation Laboratory at the ETH Zürich, to Robert Hofmann, whose technical assistance was crucial, to Ruud Weijermars for comments on an earlier version of the manuscript, and to Stefan Schmid and Martin Casey for many stimulating discussions on the subject of fold development.

REFERENCES

Biot, M. A. 1957. Folding instability of a layered viscoelastic medium under compression. *Proc. R. Soc. Lond.* **A242**, 444–454.

Biot, M. A. 1959a. Folding of a layered viscoelastic medium derived from an exact stability theory of a continuum under initial stress. *Appl. Math. Q.* **17**, 185–204.

Biot, M. A. 1959b. On the instability and folding deformation of a layered viscoelastic medium in compression. *J. appl. Mech.* **E26**, 393–400.

Biot, M. A. 1961. Theory of folding of stratified viscoelastic media and its implications in tectonics and orogenesis. *Bull. geol. Soc. Am.* **72**, 1595–1620.

Biot, M. A., Odé, H. & Roever, W. L. 1961. Experimental verification of the theory of folding of stratified viscoelastic media. *Bull. geol. Soc. Am.* **72**, 1621–1632.

Casey, M. & Huggenberger, P. 1985. Numerical modelling of finite-amplitude similar folds developing under general deformation histories. *J. Struct. Geol.* **7**, 103–114.

Chapple, W. M. 1968. A mathematical theory of finite-amplitude rock-folding. *Bull. geol. Soc. Am.* **79**, 47–68.

Cobbold, P. R. 1975. Fold propagation in single embedded layers. *Tectonophysics* **27**, 333–351.

Fletcher, R. C. 1974. Wavelength selection in the folding of a single layer with power-law rheology. *Am. J. Sci.* **274**, 1029–1043.

Fletcher, R. C. 1977. Folding of a single viscous layer: exact infinitesimal-amplitude solution. *Tectonophysics* **39**, 593–606.

Fletcher, R. C. & Sherwin, J. 1978. Arc lengths of single layer folds: a discussion of the comparison between theory and observation. *Am. J. Sci.* **278**, 1085–1098.

Ghosh, S. K. 1966. Experimental tests of buckling folds in relation to strain ellipsoid in simple shear deformation. *Tectonophysics* **3**, 169–185.

Hubbert, M. K. 1937. Theory of scale models as applied to the study of geologic structures. *Bull. geol. Soc. Am.* **48**, 1459–1520.

Hudleston, P. J. 1973. An analysis of 'single-layer' folds developed experimentally in viscous media. *Tectonophysics* **16**, 189–214.

Mancktelow, N. S. 1988a. An automated machine for pure shear deformation of analogue materials in plane strain. *J. Struct. Geol.* **10**, 101–108.

Mancktelow, N. S. 1988b. The rheology of paraffin wax and its usefulness as an analogue for rocks. *Bull. geol. Instn. Univ. Uppsala* **14**, 181–193.

Manz, R. & Wickham, J. 1978. Experimental analysis of folding in simple shear. *Tectonophysics* **44**, 79–90.

Neurath, C. & Smith, R. B. 1982. The effect of material properties on growth rates of folding and boudinage: experiments with wax models. *J. Struct. Geol.* **4**, 215–229.

Ramberg, H. 1963. Fluid dynamics of viscous buckling applicable to folding of layered rocks. *Bull. Am. Ass. Petrol. Geol.* **47**, 484–515.

Ramberg, H. 1981. *Gravity, Deformation and the Earth's Crust* (2nd edn). Academic Press, London.

Ramsay, J. G. & Huber, M. I. 1987. *The Techniques of Modern Structural Geology. Volume 2: Folds and Fractures*. Academic Press, London.

Sherwin, J. & Chapple, W. M. 1968. Wavelengths of single layer folds: a comparison between theory and observation. *Am. J. Sci.* **266**, 167–179.

Smith, R. B. 1975. Unified theory of the onset of folding, boudinage and mullion structure. *Bull. geol. Soc. Am.* **86**, 1601–1609.

Smith, R. B. 1977. Formation of folds, boudinage, and mullions in non-Newtonian materials. *Bull. geol. Soc. Am.* **88**, 312–320.

Smith, R. B. 1979. The folding of a strongly non-Newtonian layer. *Am. J. Sci.* **279**, 272–287.

Treagus, S. H. 1973. Buckling instability of a viscous single-layer

system, oblique to the principal compression. *Tectonophysics* **19**, 271–289.

Tullis, J. A. 1979. High temperature deformation of rocks and minerals. *Rev. Geophys. (Space Phys.)* **17**, 1137–1154.

Tullis, T. E. & Tullis, J. 1986. Experimental rock deformation techniques. In: *Mineral and Rock Deformation: Laboratory Studies—The Paterson Volume* (edited by Hobbs, B. E. & Heard, H. C.). *Am. Geophys. Un. Geophys. Monogr.* **36**, 297–324.

Weijermars, R. & Schmeling, H. 1986. Scaling of Newtonian and non-Newtonian fluid dynamics without inertia for quantitative modelling of rock flow due to gravity (including the concept of rheological similarity). *Phys. Earth & Planet. Interiors* **43**, 316–330.

Williams, J. R., Lewis, R. W. & Zienkiewicz, O. C. 1978. A finite-element analysis of the role of initial perturbations in the folding of a single viscous layer. *Tectonophysics* **45**, 187–200.